# Drying-Mediated Assembly of Colloidal Nanoparticles into Large-Scale Microchannels

**Wei Han, Bo Li, and Zhiqun Lin***

School of Materials Science and Engineering, Georgia Institute of Technology, Atlanta, Georgia 30332, United States

**ABSTRACT** Large-scale highly ordered microchannels were spontaneously and rapidly created by simply drying the colloidal nanoparticle suspension on a rigid substrate. Interestingly, free evaporation of colloidal suspension yielded radially aligned microchannels, while constrained evaporation that was rendered by the use of confined geometries composed of either two nearly parallel plates or a slide placed perpendicular to a rigid substrate imparted the formation of periodic arrays of parallel microchannels in a controllable manner. The microchannels were formed as a result of the competition between stress relaxation due to crack opening that ruptured the film and stress increase due to the loss of solvent. Quite intriguingly, these patterned microchannels can be exploited as templates to craft well-ordered metallic stripes. This facile and scalable approach may offer a new paradigm of producing microscopic patterns over large areas with unprecedented regularity at low cost that can serve as scaffolds for use in microelectronics and microfluidic-based biochips, among other areas.

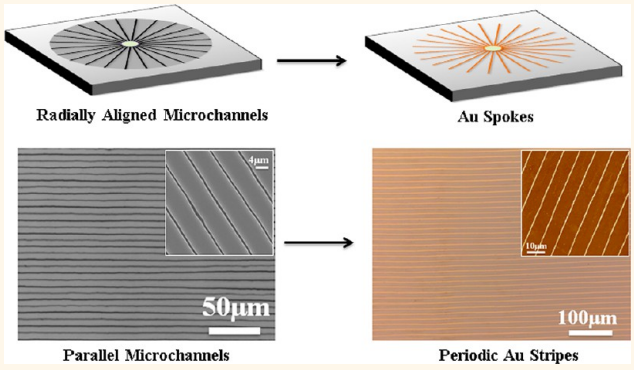


**KEYWORDS:** colloidal suspension · drying-mediated assembly · cracks · microchannels

Surface patterning is of great interest and technological importance to realize the potential of assembled structures for use in microelectronics,[1] optoelectronics,[2] microfluidic devices,[3] and biotechnology.[4] In comparison to conventional top-down patterning techniques (*e.g.*, photolithography, e-beam lithography, soft lithography, and nanoimprint lithography), due to its simplicity, high yield, and ease of implementation over large areas, self-assembly is an efficient bottom-up approach to direct small building blocks and materials into desired patterns and structures, thereby providing a lithography- and external-field-free means of producing highly ordered, often intriguing structures.[5] Among a variety of self-assembly processes, dynamic self-assembly of nonvolatile solutes *via* irreversible solvent evaporation from a substrate has been recognized as an extremely simple and emerging technique to explore the full extent of drying process for patterning surfaces with particles, polymers, DNA, *etc.* into a wide range of complex ordered structures in a simple and inexpensive manner.[6−17]

Colloidal particles dispersions with a liquid phase solvent self-assemble into a multitude of ordered structures upon drying. Recently, various methods have been adopted for structuring particles on a flat substrate, including controlled evaporative self-assembly,[18,19] surface modification,[20] and template-directed assembly.[21] In addition to controllably assembling and positioning colloidal particles into well-ordered stripes or 2D arrays,[19] cracks formed during the drying of colloidal suspension has received considerable attention because of its importance in numerous applications, such as paints, wet clays, ceramic coatings, glazes, and so forth.[22−26] These cracks exhibit intriguing morphologies, including 2D network and logarithmic spirals.[27,28] The crack formation has been widely studied theoretically, and models were developed to describe the qualitative features of crack morphology (*e.g.*, the crack spacing scales with the film thickness, and there exists a critical stress to form cracks) and the facture mechanism;[24,29] by contrast, there are far less research focused on the control over directional cracks and

* Address correspondence to zhiqun.lin@mse.gatech.edu.

Received for review April 16, 2013 and accepted June 3, 2013.

**Published online June 03, 2013**
**10.1021/nn401885f**

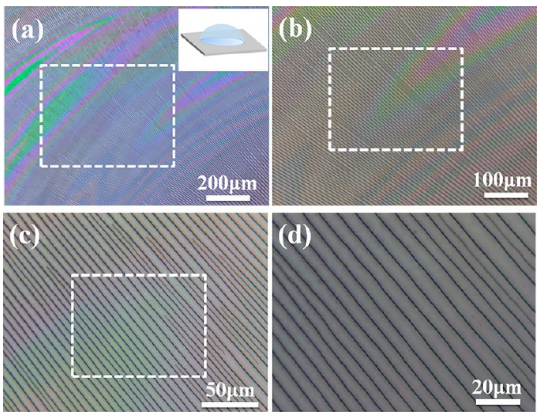


**Figure 1. Optical micrographs of highly ordered spoke-like microchannels on the Si substrate at different magnifications. The dashed boxes in panels a, b, and c correspond to the close-up optical micrographs in panels b, c, and d, respectively. A schematic representation of drying PS nanoparticle suspension on a Si substrate is shown as an inset in panel a.**

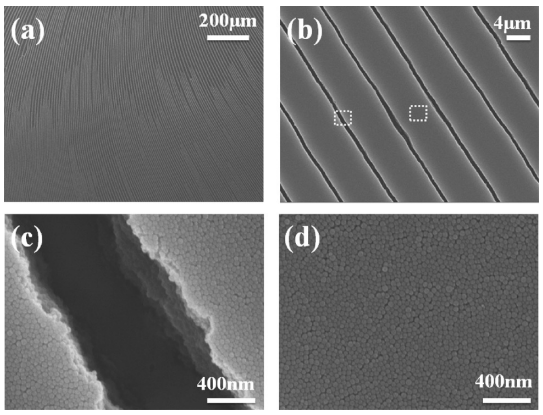


**Figure 2. (a and b) Typical SEM images of microchannels (*i.e.*, cracks) formed on the Si substrate at different magnifications. The left and right dashed boxes in panel b correspond to the close-up images in panels c and d, respectively. (c) SEM image showing that the edge of cracks was very sharp. (d) SEM image of closely packed PS nanoparticles on the surface of microscopic PS patterns.**

the constrained evaporation on the formation and propagation of cracks. Moreover, the use of cracks as templates to yield inorganic stripes has not yet been explored.

Herein, we report spontaneous and rapid formation of highly ordered microchannels over a large area by drying-mediated self-assembly of colloidal nanoparticles. Interestingly, radially aligned microchannels were yielded from freely evaporating colloidal suspension, while periodic arrays of parallel microchannels were created *via* the constrained evaporation rendered by the use of confined geometries composed of either two nearly parallel plates or a slide placed vertical to a rigid substrate. The formation of microchannels was a direct consequence of the competition between stress relaxation due to crack opening that fractured the film and stress increase due to the loss of solvent. Subsequently, the microchannels were exploited as templates to form highly regular Au stripes. This fast, simple and scalable approach may open a new avenue for producing microscopic patterns that can be readily employed as scaffolds for use in microelectronics, optoelectronics, microfluidic devices, and biochip-based detection.

## RESULTS AND DISCUSSION

The PS latex nanoparticles (diameter, $D$ = 50 nm,) were chosen as building blocks to prepare surface patterns. A drop of PS latex particle suspension (volume, $V$ = 15 $\mu$L; concentration, $c$ = 1.0 wt %) on a Si substrate was allowed to freely evaporate. To promote the evaporation of water, the suspension was heated at 60 °C by placing the Si substrate on the heating plate. Previously, we reported the formation of concentric coffee rings of PS nanoparticles due to controlled and repetitive "stick−slip" motion of the three-phase contact line *via* confined evaporative self-assembly of PS nanoparticle *solution* at very low concentration ($c$ = 0.01 wt %).[19] By contrast, the use of highly concentrated PS nanoparticle *suspension* ($c$ = 1.0 wt %) yielded intriguing well-ordered spoke-like patterns (*i.e.*, dark lines) over a large area on the Si substrate after complete water evaporation (Figure 1). It has been demonstrated that there exists a critical thickness (proportional to $c$) below which cracks do not occur.[26] The heated substrate enhanced the water evaporation, thus making the completion of evaporation process in less than 5 min. Remarkably, the entire pattern was formed over a 6 × 6 mm$^2$ surface area and the representative optical micrograph only showed a small zone of it. It is noteworthy that these spokes extended from the edge to the center of the pattern without intersecting each other. Locally, they appeared as parallel stripes (Figure 1c,d). It is interesting to note that the spoke-like surface patterns were highly reproducible (the experiments were repeated under same conditions for more than 50 times).

To scrutinize the surface morphology and the packing of PS nanoparticles, scanning electron microscope (SEM) measurements were performed (see Experimental Methods). Clearly, the dark spokes seen in Figure 1 were microscopic channels (*i.e.*, cracks) with approximately 1 $\mu$m wide as revealed by SEM (Figure 2b,c); they were separated by the arrays of PS nanoparticle patterns with a width of 6.4 ± 0.2 $\mu$m as shown in the representative SEM image (Figure 2b). The edge of cracks was very sharp; the PS pattern was composed of more than 10 layers of nanoparticles (Figure 2c). The formation of microchannels (*i.e.*, cracks) was resulted from the competition between the stress relaxation due to the crack opening that fractured the film and the stress increase from the evaporative loss of water.[22] Within the microscopic PS patterns, highly close-packed nanoparticles with small surface roughness were

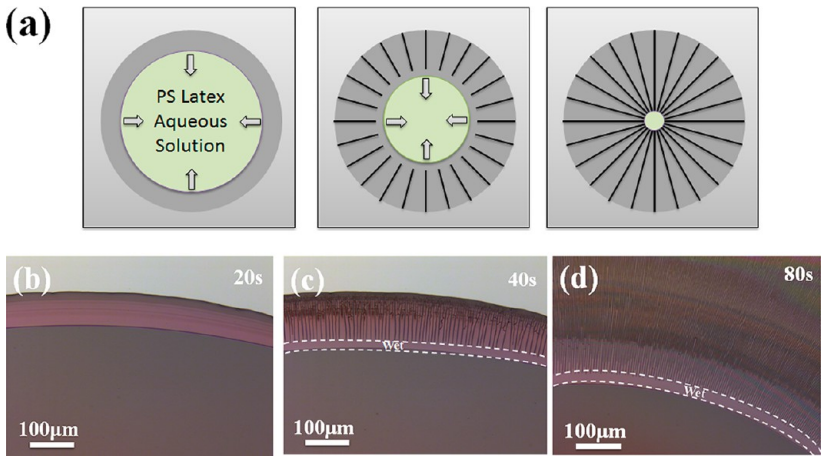


**Figure 3. (a) Schematic stepwise representation of the formation of microchannels (*i.e.*, cracks) *via* drying-mediated self-assembly of highly concentrated PS nanoparticle suspension. (b–d) Optical micrographs of drying front taken at different times ((b) 20 s, (c) 40 s and (d) 80 s) from the *in situ* optical microscopy measurement. The wet region was marked (*i.e.*, "wet") within two dashed curves in panels c and d.**

observed (Figure 2d) as a result of the rapid descending of liquid/air interface that pushed the nanoparticles down during the fast water evaporation process.[30] The cross-sectional analysis of AFM height images revealed that these microchannels had a relative depth of approximately 400 nm (see Supporting Information, Figure S1). However, as the AFM tip may not reach the bottom of cracks, in order to determine the real depth of cracks, the sample was prepared on the glass substrate under the same experimental condition (*e.g.*, same concentration, loading volume and heating temperature). Notably, the cracks were also clearly observed on the back side of the sample (Figure S2), suggesting that the cracks penetrated all the way down to the glass substrate. Thus, the crack depth was equal to the local thickness of the PS pattern (ranging from 3 to 7 $\mu$m measured by Dektak profilometer, corresponding to the location from the edge to the center of PS nanoparticle film (Figure S3)). Moreover, the spacing between the cracks was found to be simply proportional to the film thickness, which was consistent with previous theoretical studies.[22] The cracks first appeared on the surface of the deposited PS film, subsequently propagated to the interior of the film, and finally penetrated the whole film to the substrate.[31] As such, these cracks make them promising candidate as templates to create inorganic patterns.

We now turn our attention to further address qualitatively the formation of microchannels (*i.e.*, cracks) based on our *in situ* optical microscopy observation. First, the evaporation of water concentrated the PS nanoparticles into a closely packed thin film (*i.e.*, drying-mediated self-assembly of nanoparticles; left panel in Figure 3a, and the corresponding optical micrograph in Figure 3b), and no cracks were observed at this stage of the drying process. Further evaporation pulled the three-phase contact line inward and generated a negative capillary pressure, $P \sim \gamma/R$ in proportion to the surface tension of water $\gamma$ and the radius of curvature of the meniscus between particles $R$,[22,30] thus putting the assembled PS nanoparticles in compression normal to the substrate and in tension in the plane of the film, as the rigid substrate (*i.e.*, Si or glass) prevented the deformation laterally.[32] If the tensile stress exceeded the yield stress of the packed nanoparticle film, the strain energy stored in the film can be released by creating new interface, thereby forming the crack (middle panel in Figure 3a, and the corresponding optical micrograph in Figure 3c).[30] As the drying front moved inward due to the continued evaporation, the newly formed crack can serve as the nucleation site and propagate in the direction perpendicular to the drying front (*i.e.*, parallel to the drying direction).[22,23] It is worth noting that the wet region (marked "wet" in Figure 3c,d) that separated the inner suspension and outer dried film with cracks consisted of closely packed nanoparticles but with the void space between them still filled with water.[30,33] Finally, all the cracks ended and concentrated at the center of the thin PS nanoparticle film, forming spoke-like patterns globally (right panel in Figure 3a, and the corresponding optical micrograph in Figure 3d). Interestingly, the width of the wet region remained almost unchanged during the evaporation process and moved behind the drying front of colloidal suspension, indicating the propagating velocity of cracks was dependent on the moving speed of drying front (*i.e.*, drying-induced cracks).[7,22–25] With the drying front progressively moved inward, the drying-induced cracks formed in the fast evaporation process can invade the surface of deposited film,[22] penetrate the whole film,[31] and propagate inward to the center of the film, yielding well-ordered directional microchannels.

It is well-known that the surface wetting property of substrate governs the structure formation in a predictable way.[34] In this context, we prepared the samples

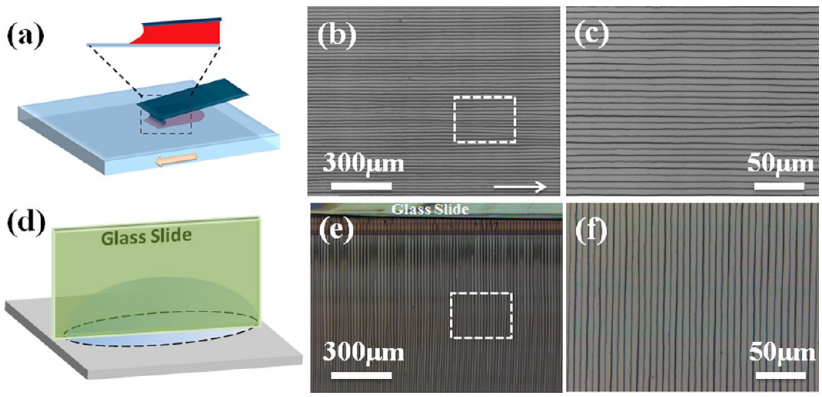


**Figure 4. Constrained evaporation in the confined geometries composed of (a) two nearly parallel plates, and (d) a slide situated vertically to a rigid substrate rendered the controllable formation of regularly spaced parallel microchannels. (b and c) Optical micrographs of periodic microchannels formed from (a). (e and f) Optical micrographs of periodic microchannels formed from (d).**

under the same experimental condition on the hydrophobic hexamethyldisilazane-coated substrate (HMDS with a contact angle of approximately 90°, as compared to the hydrophilic surface with a contact angle of 40° used previously (*i.e.*, Si substrate with the presence of thin native $SiO_X$ layer)). It is not surprising that no ordered microchannels were observed; instead, highly concentrated ring-like pattern on the HMDS substrate was obtained (Figure S4). Due to the large contact angle of PS nanoparticle suspension on the HMDS substrate, its three-phase contact line pinned throughout the entire evaporation process, thus leaving behind the ring-like deposit instead of a continuous thin film as noted above. Quite interestingly, the large but irregular cracks were also observed on the HMDS substrate due to the evaporation of residual solvent (*i.e.*, water). In addition to the substrate, the heating temperature also exerted a crucial influence on the evaporation process. In the present study, the Si substrates were heated at $T$ = 60 °C to facilitate the evaporation process and remove residual water trapped within the PS nanoparticle patterns, thus achieving cracks over large areas. When performing the drying experiment at room temperature, the evaporation rate was quite low. As a result, the spatial arrangement of cracks was no longer unidimensional; the branching (referred to as "secondary cracks") between cracks was also produced on the Si substrate due to the residual stresses in the film originated from the presence of residual water at room temperature. Thus, less ordered patterns on the Si substrate were formed (Figure S5).[22,33,35] We note that higher temperature ($T$ > 60 °C) increased the Marangoni flow caused by temperature-gradient-induced surface tension gradient within the droplet, thus breaking the uniformity of the pattern.

Compared to spoke-like microchannels obtained from free evaporation of colloidal suspension, parallel microchannels that are periodic in size, shape and spacing are highly desirable as templates for many applications. It has demonstrated that controlled evaporative self-assembly in the confined geometry allowed for the creation of a rich family of surface patterns with high regularity and fidelity.[8−10,14,34] The variation in size, shape, symmetry, and curvature of confined geometries inevitably influenced the evaporation process and the associated flow field, leading to interesting patterns with different morphologies.[34] We allowed a drop of PS nanoparticle suspension ($c$ = 1.0 wt %; $V$ = 15 $\mu$L) to evaporate in a confined geometry (*i.e.*, constrained evaporation) composed of two nearly parallel plates, where the upper plate (*i.e.*, glass slide) was fixed, while the lower plate (*i.e.*, Si substrate on a heating plate at 60 °C) was mounted on a computer-controlled translational stage that can be programed to move against the upper plate at a fixed distance (see Experimental Methods; Figure 4a). The velocity $v$ of the lower moving plate was set at a constant value ($v$ = 13 $\mu$m/s) and the separation distance between upper glass slide and lower Si substrate $H$ was fixed at $H$ = 300 $\mu$m. The evaporation time was about 5 min, depending on the moving velocity of the lower substrate (*i.e.*, $v$ = 13 $\mu$m/s in the presence study; slower moving speed required longer evaporation time). Such two-plate geometry led to straight drying front at the three phase contact line (Figure 4b, c). As the cracks were formed perpendicular to the drying front as the evaporation advanced within two-plate geometry, parallel microchannels (*i.e.*, cracks) over an impressively large area were yielded without noticeable defects (Figure 4b). Notably, parallel microchannels were also produced when imposing a glass slide in contact with a Si substrate at the center of the drop (schematic in Figure 4d, PS nanoparticle suspension, $c$ = 1.0 wt %; $V$ = 15 $\mu$L), thereby altering the shape of drying front as well. As evidenced in Figure 4e, regularly spaced channels were directed from the edge of the drop to the center glass/Si contact (marked as "Glass Slide"). It is noteworthy that the entire pattern formed by these two methods (*i.e.*, two-plate

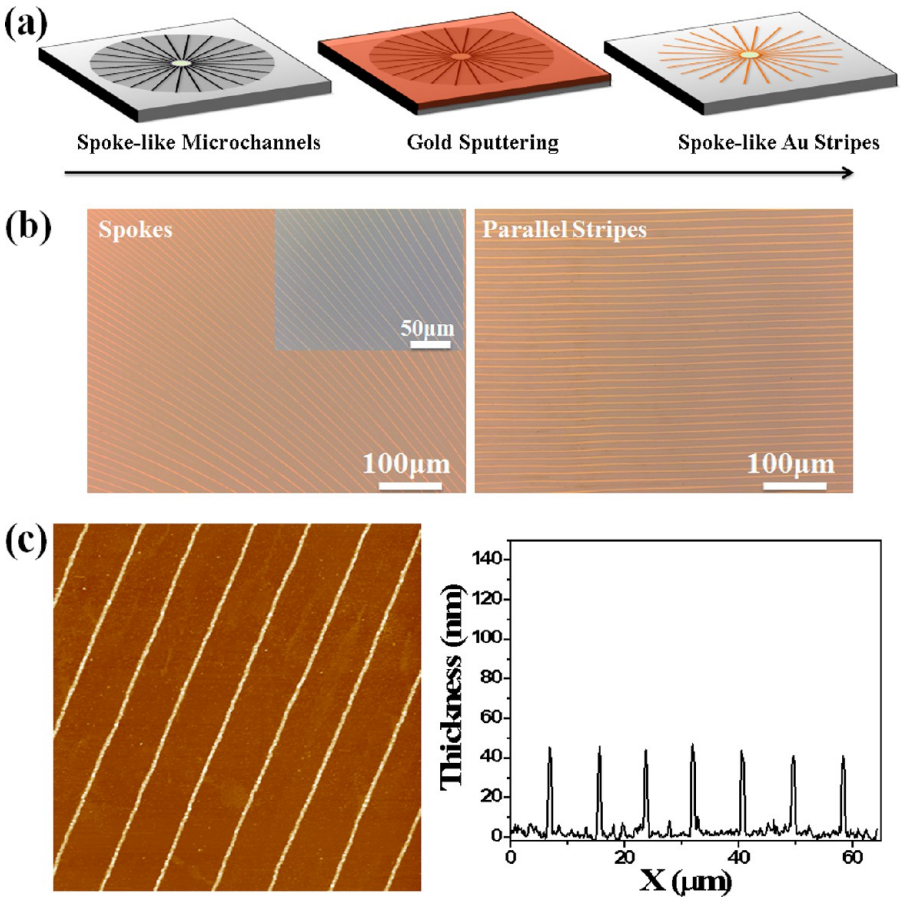


**Figure 5. (a) Schematic stepwise representation of producing Au stripes by capitalizing on spoke-like microchannels as templates. (b) Optical micrographs of spoke-like Au stripes (using templates formed by free evaporation; left) and parallel Au stripes (using templates formed by constrained evaporation between two nearly parallel plates; right). (c) Typical AFM image of parallel Au stripes, corresponding to the right optical micrograph in panel b; image size = 60 × 60 $\mu m^2$, and z range = 130 nm; the cross-sectional analysis yielded the width and height of Au stripe of 600 and 40 nm, respectively.**

and glass-slide-on- Si) was also over a 6 × 6 $mm^2$ surface area and homogeneous, as the loading volume (15 $\mu$L) in both methods was same as in the free evaporation case. These two confined geometries (two-plate and glass-slide-on- Si) may be further chemically and/or physically modified to afford an even broader range of complex ordered assembled structures with the emergence of cracks.

These highly regular microchannels can be employed as templates to produce ordered inorganic stripes. A 50 nm thick Au was sputtered on the microchannel sample (see Experimental Methods). To achieve Au stripes, the Au-coated sample was then placed in furnace at 400 °C for 2h to thermally decompose buried PS nanoparticles, followed by ultrasonication in toluene for 30 min (Figure 5a). To thoroughly remove residual PS on the surface, the thermal decomposition and ultrasonication may be conducted more than once. The optical microscope and SEM measurements clearly showed the spoke-like Au stripes and periodic parallel Au stripes were successfully obtained by capitalizing on the microchannel template created *via* free evaporation and constrained evaporation, respectively (Figure 5b and Figure S6). The order of Au stripes was reminiscent of the arrangement of microchannels and was not affected by the thermal treatment and subsequent ultrasonication. A typical AFM height image of parallel Au stripes and the corresponding cross sectional profile were shown in Figure 5c. The width and height of Au stripes were approximately 600 and 40 nm, respectively. Compared to the original width of microchannels (~1 $\mu$m), the decrease in width may be due to the long diffusion path of Au atoms into the micrometer-thick microchannels during the sputtering process as well as possible delamination of Au in the area that was adjacent to the template (*i.e.*, PS patterns) during the removal of the template.

## CONCLUSIONS

In summary, we created large-scale highly ordered microchannels in a rapid and cost-effective manner by simply subjecting the colloidal nanoparticle suspension to either freely dry on a rigid substrate or evaporate in confined geometries. The free evaporation of colloidal suspension produced spoke-like microchannels.

By contrast, constrained evaporation in confined geometries composed of either two nearly parallel plates or a slide situated vertically to a rigid substrate rendered the controllable formation of regularly spaced parallel microchannels. The formation of microchannels resulted from the competition between stress relaxation due to crack opening that broke the film and propagated inward and stress increase due to the evaporative loss of water. Importantly, these regular microchannels can be exploited as templates to produce well-ordered Au stripes. This facile and scalable approach may open up possibilities for crafting microscopic patterns over large areas with unprecedented regularity that can serve as scaffolds to yield a wide variety of inorganic arrays with different surface patterns for use in microelectronics and microfluidic-based biochips, among other areas.

## EXPERIMENTAL METHODS

**Drying-Mediated Self-Assembly of PS Nanoparticle Suspension.** The suspension containing PS latex nanoparticles with diameter of 50 nm was purchased from Thermo Scientific ($c$ = 1.0 wt % particle solids) without further purification. The Si and glass substrate was cleaned with a mixture of sulfuric acid and Nochromix, then rinsed extensively with deionized (DI) water and blow-dried with $N_2$. Hexamethyldisilazane (HMDS 99.9%) substrate was prepared by spin-coating (3000 rpm for 60s) on the Si substrate, thus changing its surface property from hydrophilic to hydrophobic. The substrate and heating plate were placed in a sealed chamber to minimize possible air convection and maintain constant temperature and humidity during the evaporation process. After the evaporation was complete, surface patterns formed on the substrates (Si, glass slide and HMDS) were examined.

**Evaporation in Two-Plate Geometry.** The confined geometry composed of two plates was constructed by placing a glass slide (*i.e.*, upper plate) nearly parallel to a Si substrate (*i.e.*, lower plate) on a heating plate at 60 °C mounted on a computer-controlled translational stage that can be programed to move against the glass slide at a fixed distance of 300 $\mu$m. The PS nanoparticle suspension ($c$ = 1.0 wt %; $V$ = 15 $\mu$L) was injected into the gap between the glass slide and the Si substrate, which was fixed on the heating plate on the linear translation stage. The velocity of the translation stage was set at a constant value ($v$ = 13 $\mu$m/s).

**Evaporation in Vertical Geometry.** The PS nanoparticle suspension ($c$ = 1.0 wt %; $V$ = 15 $\mu$L) was dropped on the heated substrate ($T$ = 60 °C) using the micropipet, and then the vertical slide was placed on top of the sessile droplet during the evaporation process.

**Template-Assisted Formation of Au Stripes.** The prepared microchannels were used as templates. Then, 50 nm-thick Au was sputtered on the template. To achieve Au stripes, the sample was then placed in a furnace at 400 °C for 2 h to thermally decompose buried PS latex particles, followed by ultrasonication in toluene for 30 min.

**Characterization.** The surface structures produced on Si substrate were characterized by optical microscopy (Olympus BX51 in the reflection mode) and atomic force microscopy (ICON scanning force microscope in the tapping mode). Vista probes (T190) with spring constants 48 N $m^{1-}$ were used as scanning probes. Surface patterns composed of PS nanoparticle film and microchannels (*i.e.*, cracks) were imaged by field-emission scanning electron microscope (FE-SEM; FEI Quanta 250) operating at 20 kV in High Vacuum. The depth of cracks was measured by Dektak 150 Profilometer.

*Conflict of Interest:* The authors declare no competing financial interest.

*Acknowledgment.* We gratefully acknowledge support from the National Science Foundation (NSF CBET-1153660 and CMMI-1153663).

*Supporting Information Available:* AFM images of PS nanoparticle film and microchannels, optical micrographs of front side and backside of microchannels on glass slide, PS nanoparticle deposits on HMDS substrate, formation of secondary cracks. This material is available free of charge *via* the Internet at http://pubs.acs.org.

## REFERENCES AND NOTES

1. Jacobs, H. O.; Whitesides, G. M. Submicrometer Patterning of Charge in Thin-Film Electrets. *Science* **2001**, *291*, 1763–1766.
2. Erdogan, B.; Song, L.; Wilson, J. N.; Park, J. O.; Srinivasarao, M.; Bunz, U. H. F. Permanent Bubble Arrays from a Cross-Linked Poly(*para*-phenyleneethynylene): Picoliter Holes without Microfabrication. *J. Am. Chem. Soc.* **2004**, *126*, 3678–3679.
3. McDonald, J. C.; Whitesides, G. M. Poly(dimethylsiloxane) as a Material for Fabricating Microfluidic Devices. *Acc. Chem. Res.* **2002**, *35*, 491–499.
4. Ostuni, E.; Chen, C. S.; Ingber, D. E.; Whitesides, G. M. Selective Deposition of Proteins and Cells in Arrays of Microwells. *Langmuir* **2001**, *17*, 2828–2834.
5. Whitesides, G. M.; Grzybowski, B. Self-Assembly at All Scales. *Science* **2002**, *295*, 2418–2421.
6. Deegan, R. D.; Bakajin, O.; Dupont, T. F.; Huber, G.; Nagel, S. R.; Witten, T. A. Capillary Flow as the Cause of Ring Stains from Dried Liquid Drops. *Nature* **1997**, *389*, 827–829.
7. Rabani, E.; Reichman, D. R.; Geissler, P. L.; Brus, L. E. Drying-Mediated Self-Assembly of Nanoparticles. *Nature* **2003**, *426*, 271–274.
8. Byun, M.; Bowden, N. B.; Lin, Z. Hierarchically Organized Structures Engineered from Controlled Evaporative Self-Assembly. *Nano Lett.* **2010**, *10*, 3111–3117.
9. Hong, S. W.; Jeong, W.; Ko, H.; Kessler, M. R.; Tsukruk, V. V.; Lin, Z. Q. Directed Self-Assembly of Gradient Concentric Carbon Nanotube Rings. *Adv. Funct. Mater.* **2008**, *18*, 2114–2122.
10. Hong, S. W.; Wang, J.; Lin, Z. Q. Evolution of Ordered Block Copolymer Serpentines into a Macroscopic, Hierarchically Ordered Web. *Angew. Chem., Int. Ed.* **2009**, *48*, 8356–8360.
11. Hong, S. W.; Xia, J. F.; Lin, Z. Q. Spontaneous Formation of Mesoscale Polymer Patterns in an Evaporating Bound Solution. *Adv. Mater.* **2007**, *19*, 1413–1417.
12. Xu, J.; Xia, J. F.; Lin, Z. Q. Evaporation-Induced Self-Assembly of Nanoparticles from a Sphere-on-Flat Geometry. *Angew. Chem., Int. Ed.* **2007**, *46*, 1860–1863.
13. Xu, J.; Xia, J. F.; Hong, S. W.; Lin, Z. Q.; Qiu, F.; Yang, Y. L. Self-Assembly of Gradient Concentric Rings *via* Solvent Evaporation from a Capillary Bridge. *Phys. Rev. Lett.* **2006**, *96*, 066104.
14. Byun, M.; Laskowski, R. L.; He, M.; Qiu, F.; Jeffries-El, M.; Lin, Z. Q. Controlled Evaporative Self-Assembly of Hierarchically Structured Regioregular Conjugated Polymers. *Soft Matter* **2009**, *5*, 1583–1586.
15. Hong, S. W.; Xu, J.; Lin, Z. Q. Template-Assisted Formation of Gradient Concentric Gold Rings. *Nano Lett.* **2006**, *6*, 2949–2954.
16. Harris, D. J.; Hu, H.; Conrad, J. C.; Lewis, J. A. Patterning Colloidal Films *via* Evaporative Lithography. *Phys. Rev. Lett.* **2007**, *98*, 148301.
17. Harris, D. J.; Lewis, J. A. Marangoni Effects on Evaporative Lithographic Patterning of Colloidal Films. *Langmuir.* **2008**, *24*, 3681–3685.
18. Yabu, H.; Shimomura, M. Preparation of Self-Organized Mesoscale Polymer Patterns on a Solid Substrate: Continuous Pattern Formation from a Receding Meniscus. *Adv. Funct. Mater.* **2005**, *15*, 575–581.

19. Han, W.; Byun, M.; Lin, Z. Assembling and Positioning Latex Nanoparticles *via* Controlled Evaporative Self-Assembly. *J. Mater. Chem.* **2011**, *21*, 16968–16972.
20. Ray, M. A.; Kim, H.; Jia, L. Dynamic Self-Assembly of Polymer Colloids To Form Linear Patterns. *Langmuir* **2005**, *21*, 4786–4789.
21. Xia, Y.; Yin, Y.; Lu, Y.; McLellan, J. Template-Assisted Self-Assembly of Spherical Colloids into Complex and Controllable Structures. *Adv. Funct. Mater.* **2003**, *13*, 907–918.
22. Allain, C.; Limat, L. Regular Patterns of Cracks Formed by Directional Drying of a Collodial Suspension. *Phys. Rev. Lett.* **1995**, *74*, 2981–2984.
23. Dufresne, E. R.; Corwin, E. I.; Greenblatt, N. A.; Ashmore, J.; Wang, D. Y.; Dinsmore, A. D.; Cheng, J. X.; Xie, X. S.; Hutchinson, J. W.; Weitz, D. A. Flow and Fracture in Drying Nanoparticle Suspensions. *Phys. Rev. Lett.* **2003**, *91*, 224501.
24. Pauchard, L.; Adda-Bedia, M.; Allain, C.; Couder, Y. Morphologies Resulting from the Directional Propagation of Fractures. *Phys. Rev. E* **2003**, *67*, 027103.
25. Shorlin, K. A.; de Bruyn, J. R.; Graham, M.; Morris, S. W. Development and Geometry of Isotropic and Directional Shrinkage-Crack Patterns. *Phys. Rev. E* **2000**, *61*, 6950–6957.
26. Tirumkudulu, M. S.; Russel, W. B. Cracking in Drying Latex Films. *Langmuir.* **2005**, *21*, 4938–4948.
27. Ngo, A. T.; Richardi, J.; Pileni, M. P. Cracks in Magnetic Nanocrystal Films: Do Directional and Isotropic Crack Patterns Follow the Same Scaling Law? *Nano Lett.* **2008**, *8*, 2485–2489.
28. Néda, Z.; Leung, K. t.; Józsa, L.; Ravasz, M. Spiral Cracks in Drying Precipitates. *Phys. Rev. Lett.* **2002**, *88*, 095502.
29. Hull, D.; Caddock, B. D. Simulation of Prismatic Cracking of Cooling Basalt Lava Flows by the Drying of Sol-Gels. *J. Mater. Sci.* **1999**, *34*, 5707–5720.
30. Smith, M. I.; Sharp, J. S. Effects of Substrate Constraint on Crack Pattern Formation in Thin Films of Colloidal Polystyrene Particles. *Langmuir* **2011**, *27*, 8009–8017.
31. Jagla, E. A. Stable Propagation of an Ordered Array of Cracks During Directional Drying. *Phys. Rev. E* **2002**, *65*, 046147.
32. Man, W.; Russel, W. B. Direct Measurements of Critical Stresses and Cracking in Thin Films of Colloid Dispersions. *Phys. Rev. Lett.* **2008**, *100*, 198302.
33. Xu, P.; Mujumdar, A. S.; Yu, B. Drying-Induced Cracks in Thin Film Fabricated from Colloidal Dispersions. *Drying Technol.* **2009**, *27*, 636–652.
34. Han, W.; Lin, Z. Learning from "Coffee Rings": Ordered Structures Enabled by Controlled Evaporative Self-Assembly. *Angew. Chem., Int. Ed.* **2012**, *51*, 1534–1546.
35. Sawadaishi, T.; Shimomura, M. Two-Dimensional Patterns of Ultra-Fine Particles Prepared by Self-Organization. *Colloids Surf., A* **2005**, *257−258*, 71–74.